Progress Toward Optical Mammography: Imaging in Dense Scattering Media Using Time-Independent Optical Sources

J. Chang[1], H. L. Graber[2], P. C. Koo[3], R. Aronson[3], S. S. Barbour[3], R. L. Barbour[1,2]

Department of [1]Pathology and [2]Biophysics, SUNY Health Science Center at Brooklyn

[3]Bioimaging Sciences Corporation 64, Burnett Terrace, West Orange, NJ 07052

ABSTRACT

Numerical studies examining the ability to reconstruct the interior properties of dense scattering media, using optical sources and analyzing surface measurements, are described. The quality of the images obtained depended on the medium, constraints, view angle, and algorithm. All algorithms produced precise location with minimal artifact from the simulation data. Restricting the view angle produced a degradation in image quality, but clearly recognizable images were obtained.

I. INTRODUCTION

Recent studies using optical laser sources have shown considerable potential for developing an alternative to x-ray mammography [1]. Because of the intense scattering of optical photons by tissue, any practical scheme must be capable of evaluating the overwhelmingly dominant multiply scattered signal.

In this paper we present image reconstruction results derived from the evaluation of two types of model media: a cylindrical phantom containing a single absorber and a 3-D MR breast phantom with added "pathologies." We consider the latter because we believe it is efficient and practical to test and systematically develop the numerical methods used in the forward and inverse computations using models that are anatomically accurate. Image recovery was accomplished by solving a system of linear perturbation equations using three iterative methods - projection onto convex set (POCS), conjugate gradient descent (CGD) and simultaneous algebraic reconstruction algorithm (SART).

II. PERTURBATION MODEL

The migration of monoenergetic photons through the medium can be described by the transport equation [2]:

$$\frac{1}{c(\mathbf{r})}\frac{\partial\phi(\mathbf{r},\Omega,t)}{\partial t} = -\Omega\cdot\nabla\phi(\mathbf{r},\Omega,t) - \Sigma_T(\mathbf{r},\Omega)\phi(\mathbf{r},\Omega,t) + \int\Sigma_s(\mathbf{r},\Omega'\to\Omega)\phi(\mathbf{r},\Omega',t)d\Omega' + s(\mathbf{r},\Omega,t) \quad (1)$$

where:

$c(\mathbf{r})$ = the speed of light.

$\phi(\mathbf{r},\Omega,t)$ = photon angular intensity at $\mathbf{r}$ with direction Ω.

$s(\mathbf{r},\Omega,t)$ = angular source density at $\mathbf{r}$ with direction Ω.

$\Sigma_s(\mathbf{r},\Omega\to\Omega')$ = macroscopic angular scattering cross section at $\mathbf{r}$ from direction Ω into direction Ω'.

$\Sigma_s(\mathbf{r},\Omega)$ = macroscopic angular scattering cross section.

$\Sigma_a(\mathbf{r},\Omega)$ = macroscopic angular absorption cross section.

$\Sigma_T(\mathbf{r},\Omega) = \Sigma_s(\mathbf{r},\Omega) + \Sigma_a(\mathbf{r},\Omega)$ = macroscopic angular total cross section.

Symbolically:

$$L\phi = s, \quad (2)$$

where L is an integrodifferential operator. Let the optical properties and angular intensity be perturbed. Then the transport equation becomes:

$$(L + \Delta L)(\phi + \Delta\phi) = s,$$
$$L\Delta\phi = s - L\phi - \Delta L\phi - \Delta L\Delta\phi = -\Delta L\phi - \Delta L\Delta\phi. \quad (3)$$

If the second order term $\Delta L\Delta\phi$ can be ignored:

$$L\Delta\phi = -\Delta L\phi. \quad (4)$$

That is, if ϕ is the solution satisfying the boundary conditions with source s, then $\Delta\phi$ is the solution satisfying the same boundary conditions with source:

$$s' = -\Delta L\phi. \quad (5)$$

Let $G(\mathbf{r}_1,\Omega_1;\mathbf{r}_2,\Omega_2;t)$ be the Green's function satisfying the transport equation for the reference medium, and apply a well–known reciprocity theorem. Then the solution of the perturbation equation is:

$$\Delta\phi(\mathbf{r},\Omega,t) = \int_V\int_{4\pi}\Delta\Sigma_T(\mathbf{r}',\Omega')w_T(\mathbf{r},\Omega;\mathbf{r}',\Omega';t)d\Omega'\,d^3r' + \int_V\int_{4\pi}\int_{4\pi}\Delta\Sigma_s(\mathbf{r}',\Omega''\to\Omega')w_s(\mathbf{r},\Omega;\mathbf{r}',\Omega''\to\Omega';t)d\Omega''d\Omega'\,d^3r' \quad (6)$$

where

$$w_T(\mathbf{r},\Omega;\mathbf{r}',\Omega';t) = -\int_V\int_{4\pi}s(\mathbf{r}'',\Omega'',t)\otimes G(\mathbf{r}',\Omega';\mathbf{r}'',\Omega'';t) \otimes G(\mathbf{r}',-\Omega';\mathbf{r},-\Omega;t)d\Omega''\,d^3r''$$

$$w_s(\mathbf{r},\Omega;\mathbf{r}',\Omega''\to\Omega';t) = \int_V\int_{4\pi}s(\mathbf{r}''',\Omega''',t)\otimes G(\mathbf{r}',\Omega'';\mathbf{r}''',\Omega''';t) \otimes G(\mathbf{r}',-\Omega';\mathbf{r},-\Omega;t)d\Omega'''\,d^3r'''$$

are called the weight functions.

The results to be presented below all were obtained in cases in which the optical properties of the medium were isotropic: $\Sigma_a(\mathbf{r},\Omega) = \Sigma_a(\mathbf{r})$, $\Sigma_s(\mathbf{r},\Omega) = \Sigma_s(\Omega)$. We further assumed that only the absorption cross sections were perturbed and only continuous wave (CW) sources were used. Under these assumptions, the solution of the perturbation

0-7803-2544-3/95 $4.00 © 1995 IEEE

equation can be obtained by Fourier transforming Eq. (6) and setting the frequency ω to 0:

$$\Delta\bar{\phi}(\mathbf{r}_d,\Omega_d) = \int_V \Delta\Sigma_a(\mathbf{r}')\,\bar{w}_a^{CW}(\mathbf{r}_d,\Omega_d;\mathbf{r}')\,d^3r' \qquad (7)$$

where:

$$\bar{w}_a^{CW}(\mathbf{r}_d,\Omega_d;\mathbf{r}') = \int_{4\pi} \bar{G}(\mathbf{r}',\Omega';\mathbf{r}_S,\Omega_S;0)\bar{G}(\mathbf{r}',-\Omega';\mathbf{r}_d,-\Omega_d;0)\,d\Omega'$$

and $(\mathbf{r}_S,\Omega_S)$ and $(\mathbf{r}_d,\Omega_d)$ are the source and detector location and direction. Eq. (7) can also be represented in digitized matrix form as:

$$\mathbf{W}\Delta\Sigma_a = \Delta\Phi, \qquad (8)$$

The inverse problem can be stated as follows: given a set of source-detector pairs, the perturbed detector readings (angular intensities) $\Delta\Phi$ and the pre–calculated weight function $\mathbf{W}$, find the perturbation of the macroscopic absorption cross sections $\Delta\Sigma_a$ of the target medium.

III. METHODS

Cylindrical Phantom

The numerical studies employed Monte Carlo methods to compute the internal light distributions and the flux of light re-emitted across the surface of 3–D cylindrical, homogeneous, isotropically scattering media. The cylinder axis was infinitely long, and its diameter was 20 mean free pathlengths (mfp). The heterogeneity was a single 2–mfp–diameter rod whose axis was halfway between the cylinder axis and the boundary (Figure 1A). The light source was a pencil beam directed normally to the surface, and detector readings were calculated for three different locations of the source (Figure 1B).

In the simulation, each photon incident on a medium underwent repeated scattering until it was either absorbed in the interior or escaped. Detector readings were calculated by counting all photons emerging from the cylinder within a patch of surface whose area was $5\pi/9$ mfp^2 (*i.e.*, an uncollimated cosine detector). The detectors were spaced at 10° intervals about the cylinder (Figure 1B). Only the readings of detectors in the central band were actually used by the reconstruction algorithms.

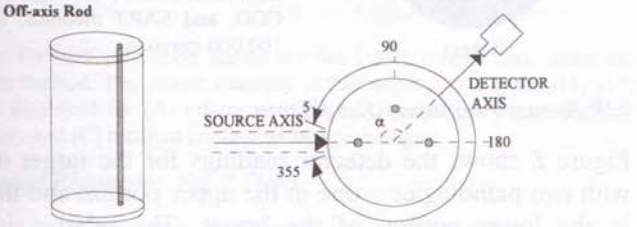

Figure 1. (A) Tissue phantoms used for Monte Carlo simulations. (B) Simulation source and detector configuration; the absorber lies at one of the three indicated locations.

3-D MR Breast Phantom

A series of sagittal MR breast images was obtained using GE Signa MR system. The fast spin echo (with T_R = 4000 msec, T_E = 112 msec, 3 mm thickness) technique was used with and without fat and water saturation. Surface coils were also used, to obtain better uniformity of the field. Figure 2A shows a sagittal section through one such image. This series of sagittal sections was then used as the reference medium in image reconstructions of the entire 3–D breast volume, a 49×35×24 array of voxels. The breast was segmented into two different tissue types – fat and parenchyma. The segmentation was done using simple thresholding. Figure 2B shows a sagittal section of a segmented image. Each tissue type was then assigned a set of optical properties – Σ_a and Σ_s. A pathology was introduced by assigning different Σ_a and Σ_s values to selected voxels. Two sets of optical properties were used, as listed in Table 1. The first set has two types of pathology – one with an absorber at the center of the breast (Figure 3A) and the other with two absorbers in upper and lower portions of the breast (Figure 3B). The second set has only one type of pathology, with absorbers in upper and lower portions of the breast (Figure 3B).

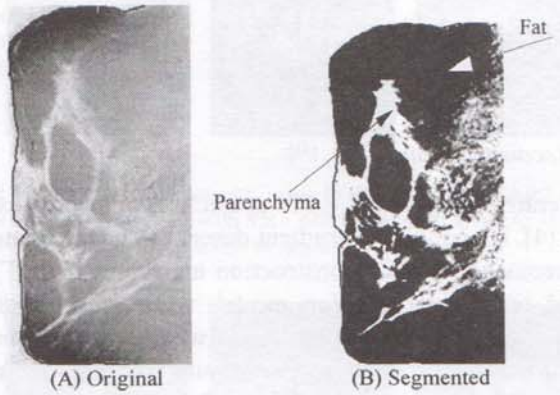

Figure 2. Illustration of segmentation of one sagittal cut of MR breast images. (A) Original MR image. (B) Segmented MR image. The fat and parenchyma tissues were segmented using simple thresholding.

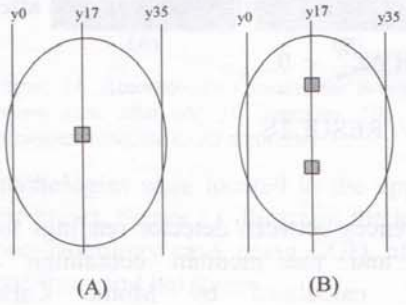

Figure 3. Illustration of the locations of two types of pathology introduced in the breast phantom. (A) One pathology at the center of the breast. (B) Two pathologies in the upper and lower portions of the breast.

	Set 1			Set 2		
	Fat	Par	Path.	Fat	Par	Path.
Σ_a	0.01	0.03	0.50	0.01	0.03	0.50
Σ_s	1.00	0.50	3.00	2.00	1.00	6.00

Table 1. Two sets of optical cross sections (Σ_a and Σ_s) assigned to phantoms reconstructed from series of MR breast images. Par = parenchyma, Path. = pathology. The dimension of Σ_a and Σ_s are mm^{-1}.

The 3–D MR breast data was used as the medium for the relaxation code. Relaxation [3] is a numerical method used to

solve the diffusion equation – an approximation to the transport equation. The continuous diffusion equation with inhomogeneous diffusion constant $D(\mathbf{r})$ is:

$$\frac{1}{c_n}\frac{\partial}{\partial t}\Phi(\mathbf{r},t) - \nabla\cdot[D(\mathbf{r})\nabla\Phi(\mathbf{r},t)] + [\Sigma_{ab} + \Sigma_a(\mathbf{r})]\Phi(\mathbf{r},t) = S(\mathbf{r},t), \quad (9)$$

where Σ_{ab} is the average, or *background*, value of the absorption cross section. Twenty sources were placed at the boundary of the breast (Figure 4A) and twenty detector readings were obtained for each source (Figure 4B), for all reference and pathological media. The photon intensity in each voxel was also recorded for the reference media in each set for weight matrix calculations.

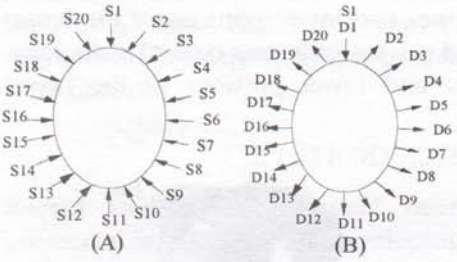

Figure 4. Illustrations of the source-detector pairs used in the study of the MR breast images: (A) twenty source locations. (B) twenty detector locations for source 1 (S1).

Image Reconstruction

Three iterative algorithms – (1) projection onto convex sets (POCS) [4], (2) conjugate gradient descent (CGD) [5], and (3) simultaneous algebraic reconstruction algorithm (SART) [6], all based on the perturbation model, were used for image reconstruction. Two range constraints were applied: positive range constraint on reconstruction results and positive range constraints on detector readings. Range constraints on detector readings were imposed prior to reconstruction, with all the negative readings set to zero: $\Delta\phi_i = 0$ if $\Delta\phi_i < 0$. The range constraints on reconstruction results were imposed after each iteration: $\Delta\Sigma_{aj}^n = 0$ if $\Delta\Sigma_{aj}^n < 0$..

IV. RESULTS

Cylindrical Phantom

Figure 5 shows the differences between detector readings for the reference medium and the medium containing a heterogeneous absorber, calculated by Monte Carlo simulations, for four different source locations. The sources entered the medium at 0°, 90°, 180° and 270° on the boundary in a single plane of the cylinder. The detectors were located every 5° on the boundary in the same plane. Only three curves are shown in this figure, since the readings for the 270° source is a mirror image of the readings from the 90° source. The curves show the largest intensity differences are obtained for the 180° source, followed by the 90° and 270° sources, and the 0° source shows the smallest intensity differences. Figure 6 shows the images reconstructed by using the data from each source separately, after 100,000 iterations of the CGD algorithm. Figure 7 shows the reconstructions obtained by using the data from all sources at once, after 100,000 iterations, using different algorithms.

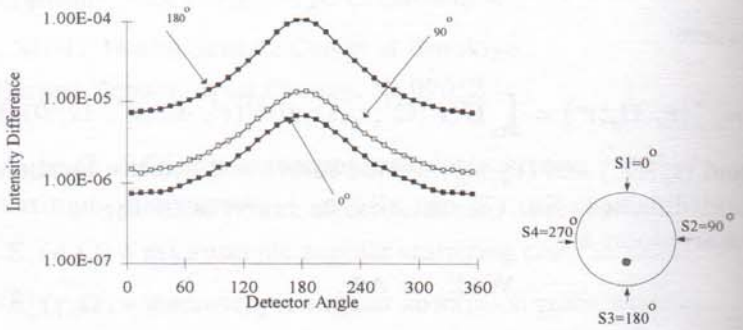

Figure 5. Monte Carlo simulation results: intensity differences $(\Delta\phi = \phi_0 - \phi)$ for off-center absorber; the 270° data is the mirror image (with respect to a vertical line at 180°) of the 90° data.

Figure 6. Reconstructed images from each individual source, using CGD, after 100,000 iterations.

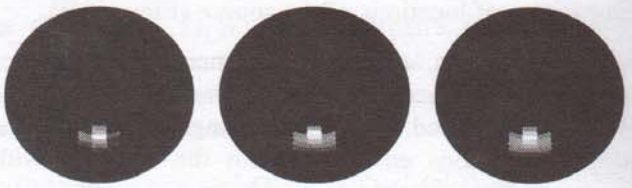

Figure 7. Reconstructed images from all four sources using POCS, CGD, and SART methods, after 100,000 iterations.

MR Breast Phantom: Set 1 Data

Figure 8 shows the detector readings for the target medium with two pathologies – one in the upper portion and the other in the lower portion of the breast. The relative intensity differences for source "S1" show one peak at the detectors opposite the source, while the relative intensity differences for source "S6" shows two peaks, and a minimum for detectors opposite the source. Figure 9 shows the forward calculation results, by displaying the photon intensity in four different sagittal cuts (y10, y15, y17 and y20) through the phantoms for

the (A) reference medium, (B) one–pathology medium, and (C) two–pathology medium. Significant changes in photon density were observed in the cuts y17 and y15. Notice that the pathologies were located in the sagittal plane y17. Figure 10 shows the reconstruction results for the one–pathology case, using the POCS, CGD and SART methods, after ten, one hundred and one thousand iterations. Figure 11 demonstrates the reconstruction results for the two–pathology case.

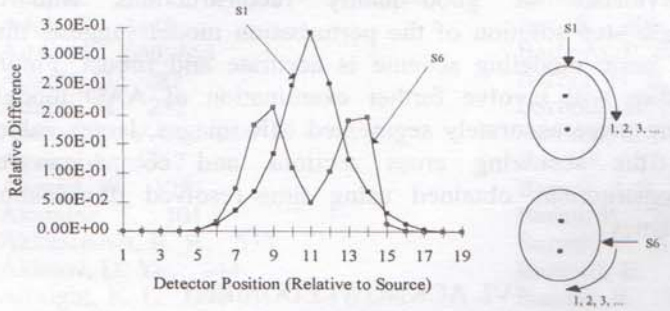

Figure 8. Simulated relative detector readings $\left(\Delta\phi/\phi_0 = 1 - \phi/\phi_0\right)$ for the medium containing two pathologies.

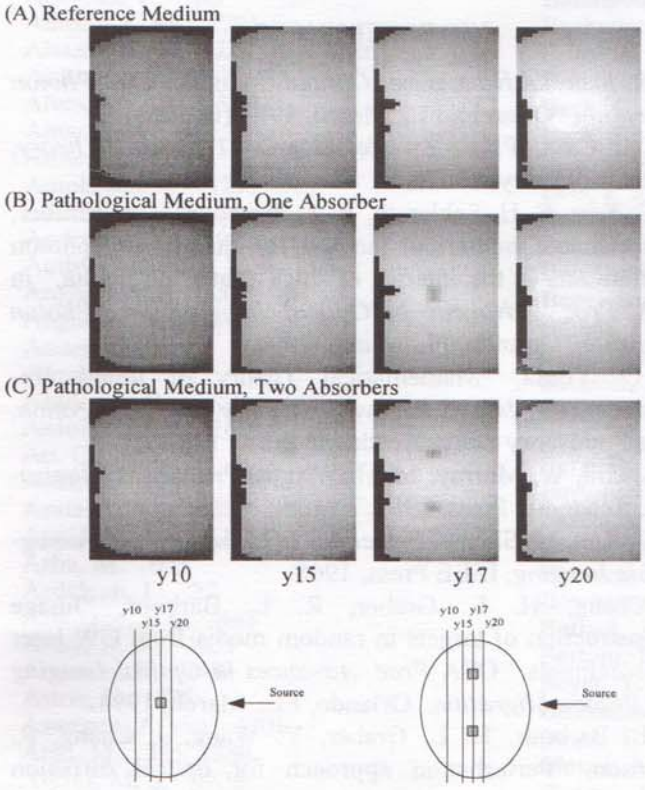

Figure 9. Forward simulation results for Set 1 MR breast data, using the relaxation method. The photon intensity in four sagittal cuts (y10, y15, y17, y20) are displayed for (A) reference medium, (B) medium containing one pathology , and (C) medium containing two pathologies.

MR Breast Phantom: Set 2 Data

Figure 12 shows the computed photon intensity in four different sagittal cuts – y10, y15, y17 and y20 – through the phantom reconstructed from the second set of MR breast data. Significant changes were observed in cuts y17 and y15. Figure 12A shows the result for the reference medium and Figure 12B that for the two–pathology medium, where two

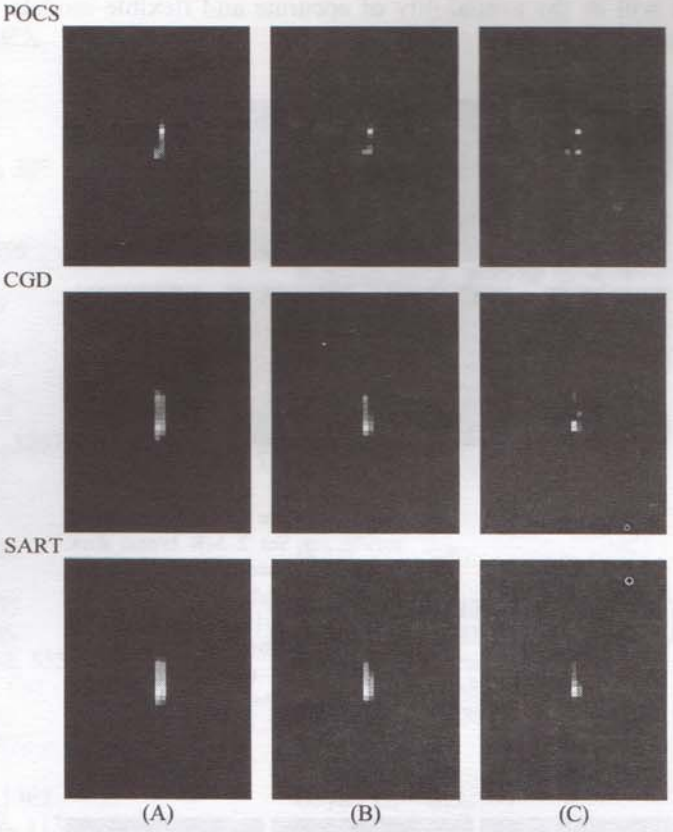

Figure 10. Reconstruction results, using POCS, CGD, and SART algorithms for the one–pathology case with Set 1 MR breast data, after (A) 10 iterations, (B) 100 iterations, and (C) 1,000 iterations.

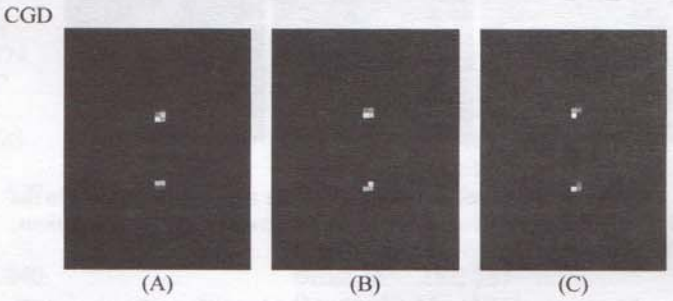

Figure 11. Reconstruction results for two–pathology case with Set 1 MR breast data, after (A) 10 iterations, (B) 100 iterations, and (C) 1,000 iterations using the CGD algorithm.

pathologies were located in the upper and lower portions of the breast. Figure 13 illustrates the images reconstructed in the two–pathology case, using CGD, after ten, one hundred, and one thousand iterations.

V. DISCUSSION AND CONCLUSIONS

Results presented here confirm and extend recent reports from our laboratory [7,8,9] that demonstrate the practical utility of adopting a linear perturbation model derived from transport theory as a scheme for imaging the interior properties of dense scattering media. We recognize that development of practical imaging schemes for medical applications will require careful evaluation of multiple parameters associated with data collection and data analysis. A key factor in this

effort will be the availability of accurate and flexible models of complex media.

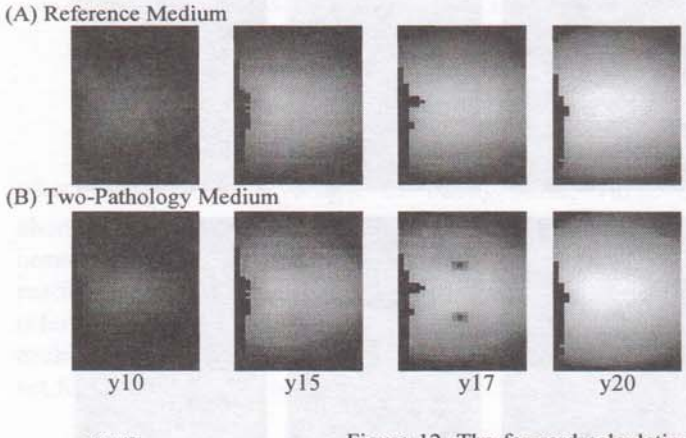

Figure 12. The forward calculation results for Set 2 MR breast data, using the relaxation method. The photon intensity in four sagittal cuts (y10, y15, y17, y20) are displayed for (A) reference medium, (B) medium containing two pathologies.

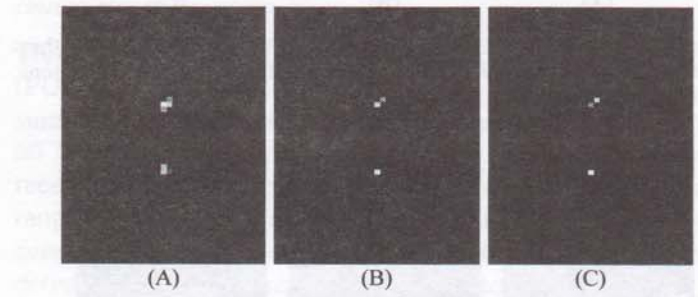

Figure 13. Reconstruction results, using CGD, for two–pathology case in the second set of MR breast images after (A) 10 iterations, (B) 100 iterations, and (C) 1,000 iterations.

In this study, we introduced the idea of evaluating MR data as a means for constructing anatomically accurate optical (AAO) models of tissue. There are many benefits to this approach. For the forward problem, evaluation of these models should permit direct evaluation of the open question of whether, under expected conditions in breast and other tissues, do solutions to the diffusion equation provide a sufficiently accurate approximation to solutions of the transport equation, or must other methods be sought? For the inverse problem, consideration of these models will allow systematic examination of the dependence of image quality, accuracy and computing times on many practical issues, including choice of algorithm, availability of *a priori* information, use of restricted view angles (*e.g.*, compressed breast), influence of noise, *etc.*

Results presented here provide a partial answer to some of these questions. Data from the cylindrical phantom demonstrated that, even in the limit of a single source, reconstruction of images that contain recognizable features of the internal structure of a random scattering medium is possible. Results obtained from analysis of MR data are particularly encouraging. Computed images directly demonstrate that accurate reconstructions can be achieved on complex media having arbitrary boundaries in the limiting case of time-independent illumination and detection.

Evidence of good–quality reconstructions with a single–step solution of the perturbation model suggests that the basic modeling scheme is accurate and robust. Future studies will involve further examination of AAO models using more accurately segmented MR images, larger values for the scattering cross sections and comparison of reconstructions obtained using time–resolved illumination schemes.

VI. ACKNOWLEDGMENT

Supported in part by NIH grant RO1–CA59955 and the New York State Science and Technology Foundation.

VII. REFERENCES

[1] OSA *Proc. Advances in Optical Imaging and Photon Migration,* Orlando, FL, March, 1994 (in press).

[2] K. M. Case, P. F. Zweifel, *Linear Transport Theory*, Addison-Wesley, 1967.

[3] P. C. Koo, F. H. Schlereth, R. L. Barbour, H. L. Graber, "An efficient numerical method for quantifying photon distributions in the interior of thick scattering media," in OSA *Proc. Advances in Optical Imaging and Photon Migration,* Orlando, FL, March, 1994.

[4] D. C. Youla, "Mathematical Theory of Image Reconstruction," *Image Recovery: Theory and Application*, edited by Henry Stark, Academic Press, 1987.

[5] P. E. Gill, W. Murray, M. H. Wright, *Practical Optimization*, Academic Press, 1981.

[6] A. V. Kak, M. Slaney, *Principles of Computerized Tomographic Imaging*, IEEE Press, 1988.

[7] J. Chang, H. L. Graber, R. L. Barbour, "Image reconstruction of targets in random media from CW laser measurements," OSA *Proc. Advances in Optical Imaging and Photon Migration,* Orlando, FL, March, 1994.

[8] R. L. Barbour, H. L. Graber, Y. Wang, J. Chang, R. Aronson, "Perturbation approach for optical diffusion tomography using continuous-wave and time-resolved data," in SPIE vol. IS11, *Medical Optical Tomography*, pp. 87-120, 1993.

[9] H. L. Graber, J. Chang, R. Aronson, R. L. Barbour "Perturbation model for imaging in dense scattering media: derivation and evaluation of imaging operators," in SPIE vol. IS11, *Medical Optical Tomography*, pp. 121-143, 1993.